Available online at www.sciencedirect.com
SCIENCE DIRECT®
Journal of Nuclear Materials 320 (2003) 54–65
journal of nuclear materials
www.elsevier.com/locate/jnucmat

Thermophysical properties of inert matrix fuels for actinide transmutation

C. Ronchi [a,*], J.P. Ottaviani [b], C. Degueldre [c], R. Calabrese [d]

[a] European Commission, Joint Research Centre, Institute for Transuranium Elements, Postfach 2340, Karlsruhe 76125, Germany
[b] Commissariat à l'Energie Atomique, DRN/DEC/SPUA, 13115 Cadarache, France
[c] Paul Scherrer Institute, 5232 Villingen, Switzerland
[d] ENEA, 40129 Bologna, Italy

Abstract

The thermal transport properties of a set of 'inert matrix fuels' (IMFs) for actinide transmutation were investigated and compared. Heat capacity, thermal diffusivity and conductivity were measured in the usable temperature range for MgO- and ZrO_2-based IMFs containing uranium, plutonium and americium, and sintered from co-precipitated or blended oxide powders.

1. Introduction

In the last decade, international cooperation programmes have been launched in several European countries with the intent of testing the technical feasibility of transmutation of minor actinides in nuclear reactors. Contrary to previous sparse experiments carried out since the 1970s, these tests are aimed at achieving higher transmutation yields, and hence are facing stringent design conditions and high performance requirements.

Within the still uncertain technological perspective of an eventual wide scale application of actinide transmutation, different possibilities are presently examined based on use of both thermal reactors (mainly in view of an 'once through' reactor irradiation strategy), and fast breeders (in the additional context of an increasingly probable fuel recycling strategy).

The choice of the materials for actinide transmutation targets is still open, the current selection criteria being based on the one hand on previous experience in conventional fuel applications, and, from the other, on the opportunity of testing innovative ad hoc materials, which might ensure a safer use of fuel rods containing high concentrations of very radiotoxic nuclides.

In this regard, refractory ceramics, especially oxides, offer a number of advantages, ranging from well-established fabrication procedures, through a generally good resistance to radiation damage, until an acceptable compatibility with the reactor coolant. In addition, in the case of a direct disposal after irradiation, several oxide fuels exhibit an excellent resistance to groundwater leaching.

The main disadvantage of oxide ceramics resides, however, in their low thermal conductivity, entailing high operation temperatures in reactor. At a first sight, this might not be a crucial problem for high melting compounds. Yet, the past experience has shown that between a low temperature irradiation regime (with high retention of helium and fission gas), and a high temperature regime (with complete in-pile fuel restructuring and high gas release, as, e.g., in LMFBR fuel) intermediate in-pile thermal conditions at high burn-up may give rise to harmful fuel/cladding mechanical interactions. In this respect, representative assessments of the rod failure risks require comprehensive in-pile tests as well as long exploratory irradiation campaigns. Alternatively,

* Corresponding author.
E-mail addresses: ronchi@itu.fzk.de (C. Ronchi), ottaviani@drncad.cea.fr (J.P. Ottaviani), claude.degueldre@psi.ch (C. Degueldre), rolando.calabrese@bologna.enea.it (R. Calabrese).

0022-3115/03/$ - see front matter © 2003 Elsevier Science B.V. All rights reserved.
doi:10.1016/S0022-3115(03)00171-5

predictions of the fuel behaviour based on defined rod design and fuel performance models are only credible if the material properties are well established. Among them, the thermal conductivity and its variation with burn-up does obviously play a primary role.

The subject of this paper deals with the thermophysical properties of fuels based on magnesium- and zirconium-oxide containing thorium, uranium, plutonium and americium, which were fabricated in the context of different projects, but have been analysed and measured in the same laboratory of the Joint Research Centre. In addition to heat capacity and thermal conductivity, other properties like expansivity, oxygen activity, effusion and melting behaviour have been also measured, though for reasons of space these results are not reported here. Actually, even the selected matter is so wide that it would be impossible to cover it exhaustively in a paper like this. The minimum we wish to have achieved is to have brought representative data in fruitful comparison.

2. Experiment

The investigated materials are listed in Table 1 together with some relevant specifications of their composition and structure. The materials were delivered to the ITU laboratory in the form of disks or pellets. Preparation of samples for thermal conductivity measurements was carried out according to a standard procedure (diamond cutting and parallel grinding with thickness variation tolerance <1%). Semitransparent samples were covered with a thin layer of carbon or tungsten, depending on the material and/or measurement temperature. All thermal treatments for the different measurements were conducted in vacuo or in a pure helium atmosphere.

The thermal conductivity, λ, was obtained as the product of the experimentally measured thermal diffusivity, α, heat capacity, C_p, and lattice density, ρ. The effect of porosity was separately calculated.

The measurements of the thermal diffusivity and of the heat capacity were carried out in the laser-flash facility LAF.I developed at ITU for very accurate measurements of the thermal transport properties of highly radioactive samples. This will make it possible to carry out in the next future comparative post-irradiation measurements of the same materials under the same conditions.

The device is installed in a lead-shielded glove box provided with remote manipulators. The sample, in the form of a disk, is heated at the measurement temperature in a HF furnace. The temperature of the sample is then slightly raised above that of the furnace by heating the bottom surface of the disk with a continuous-wave laser. This ensures that emitted or reflected thermal radiation from the HF-suscepting heater does not disturb the pyrometric measurements on the upper surface of the sample. Finally, a laser pulse is deposited onto the bottom surface of the sample; the emerging temperature perturbation on the opposite surface is recorded by a photodiode (<0.05 K sensitivity) provided with an ad hoc developed log-amplifier and integrated A/D converter, with a rise-time of the order of 10 μm s. The recorded thermogram, $\delta T = \delta T(t)$, consisting of several thousands of points, is analysed by a realistic and very precise theoretical model of the pulse propagation in the sample [1]. Thermal diffusivity, α, heat capacity, and

Table 1
Examined inert matrix fuels

Label	Matrix	Guest	Composition	Type	% th.d.	D (g cm^{-3})
A	MgO	Am	MgO:16.1wt%$Am_{1.62}$	Blended	95	3.92
B	MgO	Am	MgO:16.4wt%$Am_{2.00}$	Blended	91	3.72
C	MgO	Am	MgO:16.3wt%$Am_{1.83}$	Blended	95	3.87
D	ThO_2	U	$Th_{0.88}U_{0.12}O_2$	Blended	82.2	8.11
E	UO_2	Pu	$Pu_{0.08}$ $U_{0.92}O_{2.00}$	Blended	95	10.1/10.4
F	ZrO_2:Ca-st	U,Th	41.5 wt% ZrO_2 4.5 wt% CaO 39.2 wt% ThO_2 15.8 wt% UO_2	Blended	93.15	6.99
G	ZrO_2:Y-st	U	72.9 wt% ZrO_2 8.1 wt% CaO 19 wt% UO_2	Blended	89.9	5.59
H	ZrO_2:Er:Y-st	(Ce)	$Er_{0.07}Y_{0.10}Ce_{0.15}Zr_{0.68}O_{1.913}$	Co-precip.	89	5.7/5.8
I	ZrO_2:Er:Y-st	Pu	$Er_{0.04}Y_{0.14}Pu_{0.08}Zr_{0.74}O_{1.91}$	Co-precip.	92	5.66/5.71
L	ZrO_2:Er:Y-st	Pu	$Er_{0.04}Y_{0.14}Pu_{0.09}Zr_{0.73}O_{1.91}$	Blended	97	6.23/6.27
M	ZrO_2:Y-st	Am	$Am_{0.06}Zr_{0.78}Y_{0.16}O_{1.89}$	Blended	85	5.3
N	ZrO_2:Y-st	Am	$Am_{0.20}Zr_{0.66}Y_{0.14}O_{1.93}$	Blended	90	6.25

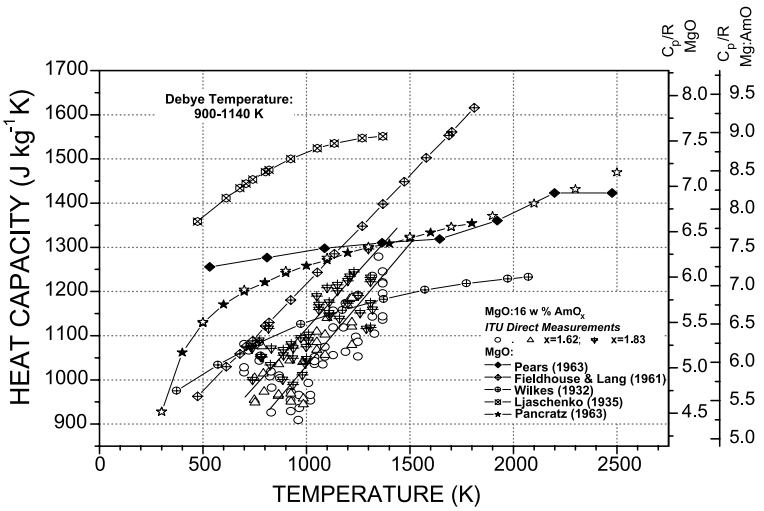

Fig. 1. Heat capacity of magnesia and magnesia–americia composite ceramics as a function of temperature.

effective heat losses are calculated numerically by an iterating numerical procedure. Different heat propagation models are respectively used for optically absorbing and semitransparent materials. For the latter, the laser probe pulse is deposited on the sample surface covered by a tungsten or carbon layer.

The precision of the measurements is normally better than 1% for α and 5% for C_p. For semitransparent samples, an independent method of calibration is necessary for evaluating C_p. When this failed, a differential scanning calorimeter (DSC) was used for heat capacity measurements.

2.1. Magnesia-based materials

2.1.1. Heat capacity of MgO

Contrary to the thermal diffusivity, whose magnitude depends on both lattice, and, possibly, on macro- and micro-structural features, the heat capacity is effectively related only to lattice and electronic properties. Therefore, the value of this quantity can be measured in suitable well-characterised samples and then applied to evaluate the specific contributions to the thermal conductivity and in structurally more complex composite materials. Yet, high temperature C_p measurements of ceramics are always difficult and often subjected to large systematic errors. Thus Pears and Osment [2], Fieldhouse and Lang [3], Ljaschenko [4,5], Pankratz and Kelley [6] and Victor and Douglas [7] measured the heat capacity of MgO at high temperature obtaining, however, a poor agreement. The results are in fact differing much more than the precision of the adopted methods would normally allow. Only in the last two references are the published $C_p(T)$ curves in good agreement, approaching the phonon saturation value of 6 R at the Debye temperature The values recommended in the JANAF tables [8] are taken from these data (Fig. 1). However, the shape of $C_p(T)$ was prefixed by fitting the temperature derivative enthalpy curves, $H = H(T)$. We cannot enter a detailed discussion of these data, we must, however, point out that thermophysical measurements in MgO at high temperature are very problematic and require a dedicated analysis [9]. For this reason, C_p measurements on pure MgO are still in progress at ITU.

The semitransparent samples of MgO:16%AmO_x were found to be more suitable for DSC than for laser-flash measurements. However, their high radioactivity produced a disturbing heat source whose influence increases with decreasing of temperature. Our results, plotted in Fig. 1, show a rather large scatter; this is because these C_p values were deduced from local numerical derivatives of the DSC curves, without previous smoothing. Compared with the above-mentioned methods, this procedure gives a more realistic view of the accuracy of the C_p measurements.

If the molar value of C_p is read on the dimensionless scale in R units, the points by Ljaschenko are the nearest to our measurements. Two samples were measured containing americium oxide with different oxygen potentials. This was measured before and after the experiments showing no significant changes. The difference in C_p between the MgO:$AmO_{1.83}$ and MgO:$AmO_{1.62}$ is of the order of 10%.

2.1.2. Thermal conductivity

The thermal diffusivity measurements of MgO:AmO_x are plotted in Fig. 2, where they are compared with those carried out on a standard sample of UO_2 ($O/U = 2.00 \pm 0.003$, 95% th.d., nuclear grade, <800 ppm impurities).

The inverse diffusivity, plotted in Fig. 3 versus T, shows an approximately linear trend. Two of the samples, especially that of intermediate stoichiometry ($AmO_{1.83}$) exhibit a more pronounced decrease of the diffusivity at high temperatures. It should be also remarked that the fitted linear slope of the inverse thermal diffusivity ranges from 500 to 550 $s\,m^{-2}\,K^{-1}$, in conjunction with a negative value of the ordinate intercept, A. The absence of a pronounced positive value of A, is in agreement with the very low solid solubility of tetra- and trivalent dopants in the MgO lattice. On the other hand, this feature may also indicate a significant temperature sensitive concentration of point defects in these materials as well as in pure MgO, whose thermal conductivity at temperatures above 700 K is not much higher than that measured in the composite oxides. The thermal conductivity versus temperature is plotted in Fig. 4.

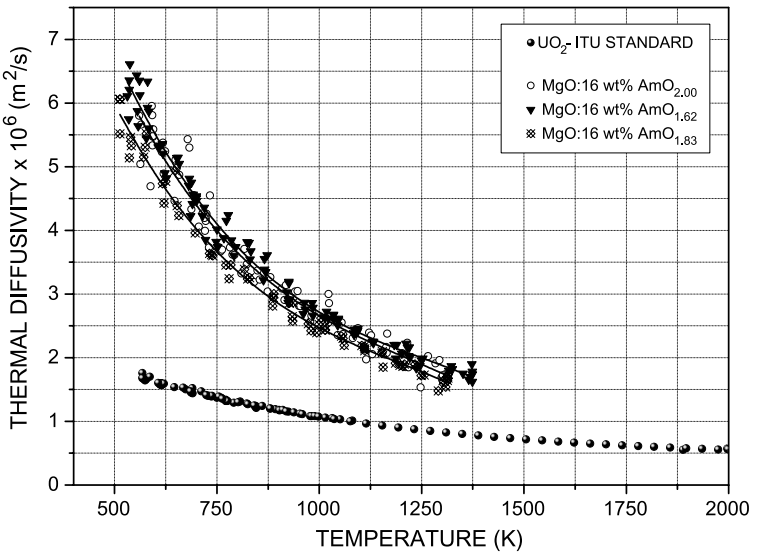

Fig. 2. Thermal diffusivity of magnesia, and magnesia–americia composites. The measurements on the UO_2 standard were conducted with the same instrument and under the same conditions as the IMFs reported in this work.

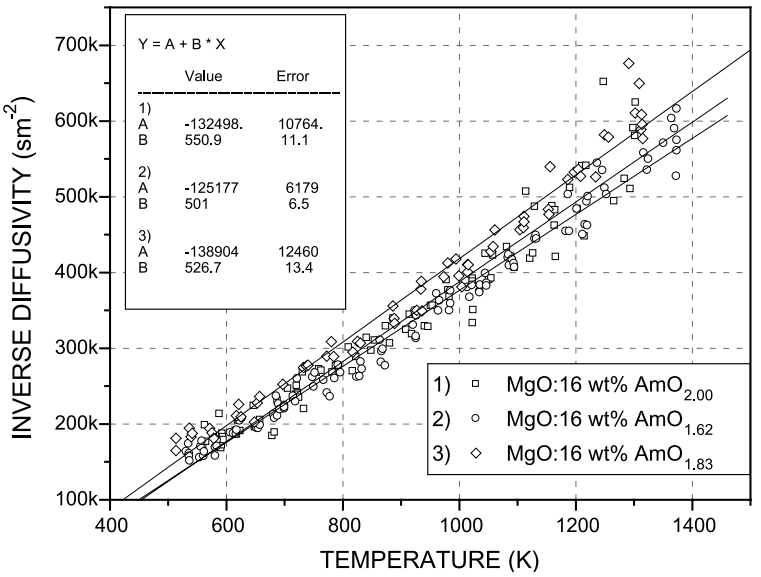

Fig. 3. Inverse diffusivity from the plot of Fig. 2. The values of the linear interpolation parameters are reported in the inset.

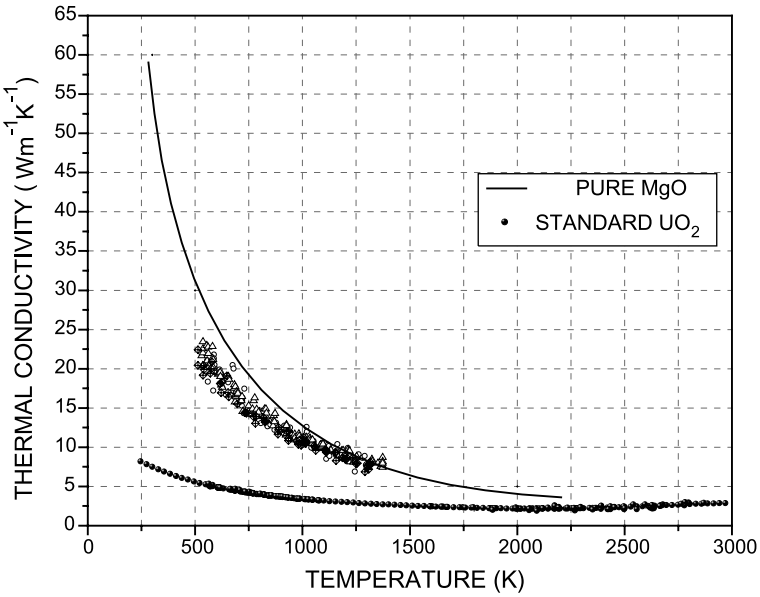

Fig. 4. Thermal conductivity of magnesia (line) and magnesia–americia composites (symbols). The latter correspond to measurements performed during repeated thermal cycling. The points at the bottom (full dots) represent thermal conductivity measurements on standard UO_2 (95% th.d.).

Finally, from the obtained results it emerges that a decrease of the oxygen activity does not significantly influence heat capacity and thermal diffusivity of MgO. In reactor applications, it is desirable that the oxygen chemical potential inside the fuel rod is kept as low as possible in order to limit cladding corrosion. This is easily achievable by fabricating, for instance, composites with a sufficiently low O/M ratio in the actinide oxide phase. Some remarks of cautions should be made, however, in this regard. In fact, whilst MgO under oxic conditions is sufficiently stable until high temperatures, under reducing conditions the equilibrium partial pressure of Mg (g) increases dramatically, so that in laboratory annealing at temperatures above 2000 K structural and geometrical instabilities are observed to occur within a few minutes [9]. For long irradiation times, this effect might create problems even at much lower temperatures. This matter is still to be carefully investigated.

2.2. Zirconia-based materials

Zirconia is no doubt an excellent matrix for actinide transmutation targets. Though all major actinides are effectively soluble in the ZrO_2 lattice, both in the pure and in the doped, cubic-stabilised form, the Zr/Ac mixed oxides exhibit eutectics at temperatures of the order of 2500 K, i.e., much higher than those predicted from simple free energy calculations [10–13]. However, except for the pure monoclinic form, crystalline zirconia has a very low thermal conductivity, which normally further decreases by lattice impurity additions.

Contrary to the case of MgO, where any type of dispersion of the AcO_x phase cannot improve the thermal properties of the IMF, in the case of zirconia some advantages may be expected by fabricating heterogeneous CERCER cellular structures, where the better conductance of the actinide inclusions may be exploited to some extent.

2.2.1. Heat capacity of ZrO_2

The experimental measurements of the heat capacity of monoclinic zirconia are rather well established in its existence temperature domain ($T < 1442$ K). The high temperature data recommended by JANAF [8] are mainly based on the values measured by Chekhovskoy and Banaev [14] and Kantor and Fomichov [15] as well as on those, somewhat lower, of Coughlin and King [16]. At higher temperatures, however, the data on both the tetragonal and cubic phase, are scanty and in part discrepant. Fig. 5 shows a plot of C_p versus T, where our measurements are compared with the available literature data. It can be seen that, in the plotted temperature range, the values of the heat capacity in the monoclinic, tetragonal, cubic and cubic-stabilised form of zirconia do not differ too much, although the molar value in the cubic-stabilised material is somewhat higher. Between 1000 and 1300 K, our measured heat capacity in YSZ increases very weakly, and this trend is maintained up to the melting temperature. However, in a series of

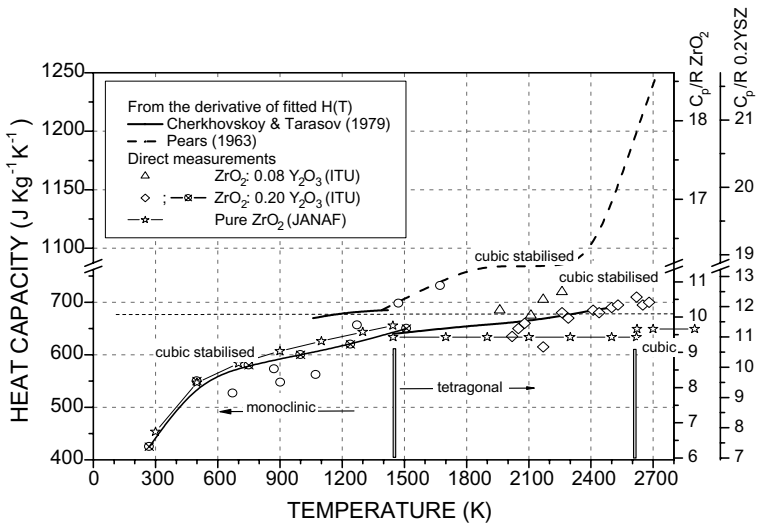

Fig. 5. Heat capacity of zirconia in different crystallographic forms as a function of temperature.

measurements conducted by Pears and Osment [2], a different trend of $C_p(T)$ was observed with an increase, between 1300 and 2600 K, from 650 to 1200 J Kg^{-1} K^{-1}.

Now, it is well known that in insulators a further increase of C_p above the n3R-value does generally result from activation of energy-absorbing mechanisms other than elastic vibrations. These may range from Mott-type electronic transitions to anharmonic effects and lattice defect formation. For instance, in UO_2 the further steep increase of C_p at temperatures above 2000 K is largely due to formation of oxygen Frenkel pairs and small polarons. However, formation of these defects entails local disproportion of the cation valence and of the ionic charge distribution. Thus, this effect is normally absent in lattices where cations have an effectively fixed valence/charge, as, e.g., in ThO_2. [1] Thus the chemical properties of Zr suggest a behaviour analogue to that of ThO_2, as in fact was confirmed by our measurements and by those of Chekhovskoy and Tarasov [14,17] on tetragonal ZrO_2 (see Fig. 5). Other high temperature measurements by Kirillin et al. [18] seem to corroborate this trend of $C_p(T)$. It remains, however, noteworthy that Pears (whose experimental method is trustworthy) measured in cubic (Ca-) stabilised zirconia a strong increase of C_p at high temperature, very similar to that observed in UO_2. We have not been able so far to confirm these measurements neither in stabilised nor in pure zirconia. Though Ackermann considered Pears measurements as spurious [19], it should be nevertheless of interest to further investigate the question whether a doped ZrO_2 crystal can be fabricated exhibiting this heat capacity behaviour. [2]

2.2.2. Thermal conductivity

Ca-st. ZrO_2:ThO_2:UO_2

These two ceramic composites have different ceramographic structures, with respectively 40% (F) and 15% (G) thoria–urania. The former exhibits a typical cellular structure with the U- and Th-rich phase surrounding dense grains of zirconia of approximately 10 μm size (Fig. 6). Material G contains 19% of isolated, globular particles of urania (Fig. 7).

The measured diffusivity is plotted in Figs. 8 and 9 for the pure Ca-stabilised material and the two composite materials F and G. The diffusivity of the mixed U–Th oxide (D) is also plotted together with that of the above-mentioned UO_2 standard. Fig. 10 shows the thermal conductivity plot versus temperature. It can be seen that the conductivity of the composite materials is in both cases very low; however, that of material G, which contains isolated urania particles, is lower than

[1] At the melting point, the excess molar heat capacity, ΔC_p, above the Neumann–Knopp value of 9 R amounts to 3.5 R in ThO_2 ($T_m = 3650$ K) against 10.7 R in UO_2 ($T_m = 3120$ K). Also PuO_2 ($T_m = 2670$ K), where plutonium can hardly assume an oxidation state higher than IV, exhibits a relatively low ΔC_p (4.8 R). According to the values plotted in Fig. 5, we have $\Delta C_p \cong 0.5$ R for pure ZrO_2 and $\Delta C_p \cong 2.5$ R for 20%-YSZ.

[2] An increase of the heat capacity due to lattice defect formation does not imply, however, a proportional increase of the conductivity since the heat spent to create defects enhances the integral phonon scattering cross section. Thus, for instance, in order/disorder first- or second-order transitions, the heat capacity diverges, while the diffusivity falls to zero due to thermodynamic fluctuations, so that the thermal conductivity is a finite, continuous function through the transition.

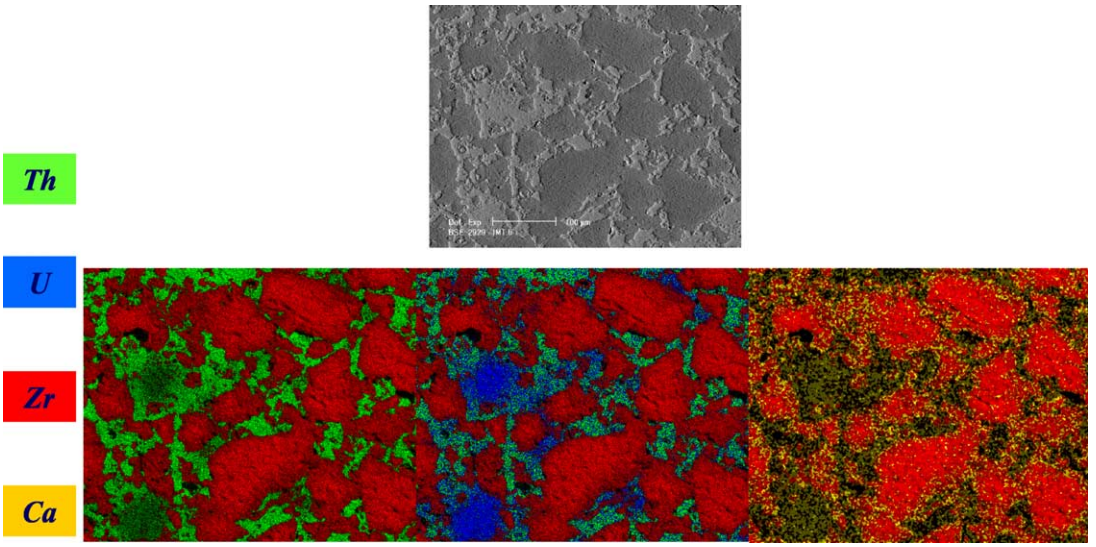

Fig. 6. Structural partition of the components in the ZrO_2–UO_2–ThO_2 composite.

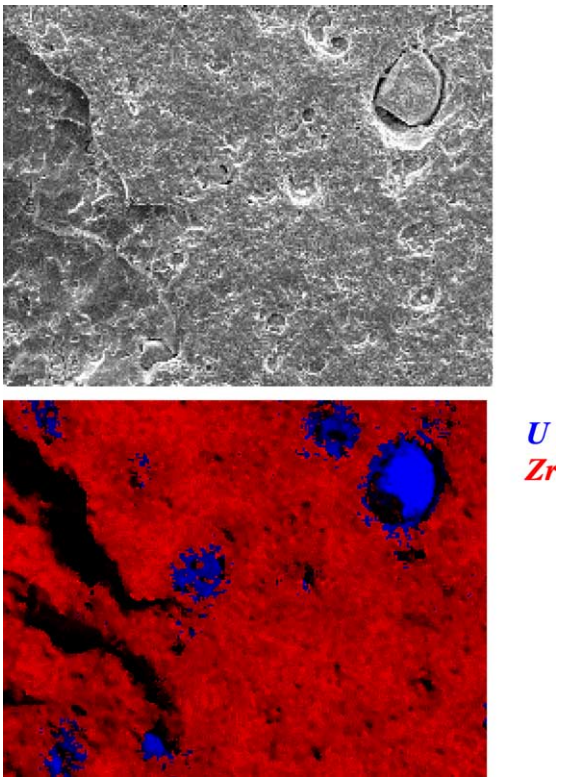

Fig. 7. Structural partition of the components in the ZrO_2–UO_2 composite.

that of the zirconia host matrix, whereas that of composite F is significantly higher.

As mentioned in the introduction, these materials are presently irradiated in the Halden reactor in instrumented capsules. From preliminary analysis of the measured in-pile centerline temperatures of the pins [20], the thermal conductivity was numerically evaluated after one-month irradiation. The results, reported in the graph, indicate a decrease of the conductivity during the first irradiation stage.

Y-st. ZrO_2:PuO_2 and Y-st. ZrO_2:AmO_x

Two zirconia-based inert matrices containing plutonium have been investigated. The first (I) is a sintered co-precipitated mixed oxide (Zr,Pu)O_2 with 16 wt% Pu, and the second (L) is a composite ceramic with the same plutonium fraction but obtained from sintered blended powers of ZrO_2 and PuO_2. The structure of the second material is cellular (Fig. 11), of the same type as that shown in the preceding section. The experiment shows (Fig. 12) that the homogeneous sample has a lower thermal diffusivity than the heterogeneous one. Furthermore, if one considers the trend of the inverse diffusivity versus T, one can realise that the thermal resistivity of the homogeneous sample increases linearly with T, whilst that of the heterogeneous sample presents at high temperature a negative deviation from the linear dependence, that is to say, a comparatively better diffusivity than in the homogeneous sample.

The inert matrix fuels (IMFs) containing americium were both sintered from mechanically blended powders of AmO_2 and $(ZrO_2)_{0.83}$ $(Y_2O_3)_{0.0085}$ with, respectively, 6 and 20 mol% Am. Americium was not completely dissolved in ZrO_2, however the actinide-rich phase was very finely dispersed (Fig. 14). The thermal diffusivity of these samples, plotted in Fig. 13 is very poor, and rather near to that of the homogeneous (Zr,Pu)O_2 compound.

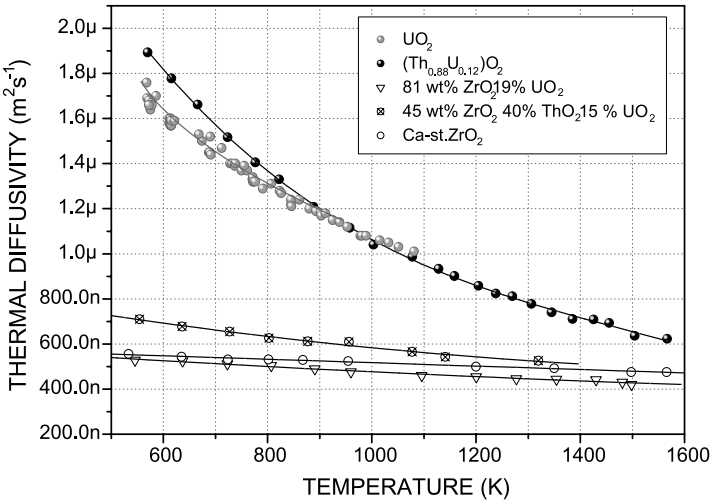

Fig. 8. Thermal diffusivity of $(U,Th)O_2$, ZrO_2–UO_2–ThO_2, and ZrO_2–UO_2 composites compared to that of Ca-stabilised ZrO_2.

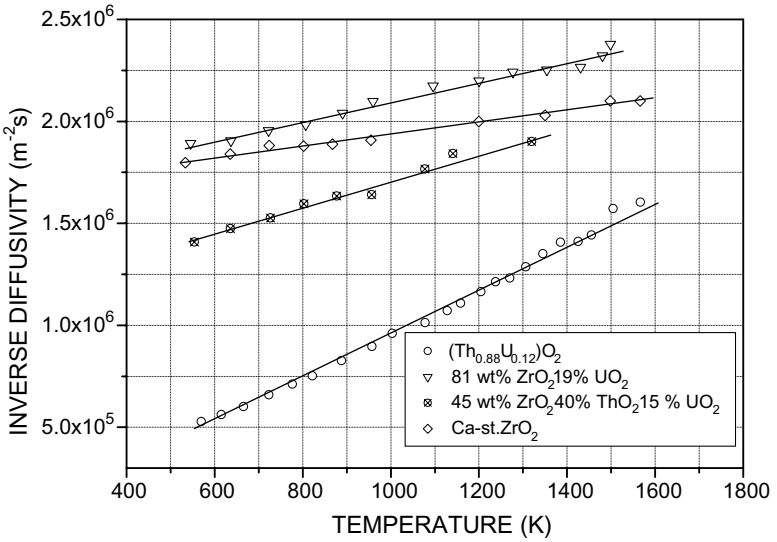

Fig. 9. Inverse diffusivity from the plot of Fig. 8.

3. Conclusions

The magnesia-based composites with a finely dispersed AmO_x phase display a good thermal conductivity, which at 500 K is only approximately ~30% lower than that of pure MgO; this difference decreases to less than 10% at temperatures above 1000 K. Due to the low solid solubility of actinides in MgO, the conductivity of this type of IMFs is only moderately affected by the grade of dispersion of the actinide phase. The stoichiometry of the AmO_x phase, which defines the oxygen chemical potential in the system, and hence has an important impact on the fuel/cladding corrosion, has no visible influence on the thermal conductivity of the composite.

The situation is essentially different for zirconia-based IMFs, where the thermal transport properties are more sensitive to the fabrication process. Fig. 15 shows a synoptic plot of the thermal conductivity, λ, of some of the examined samples compared with that of reference materials. In the explored temperature range, the conductivity values of the various zirconia-based matrices are lying between two extreme curves: that corresponding to monoclinic ZrO_2, whose conductivity is relatively high, near, e.g., to that of nuclear grade UO_2; and that of a very low conducting Y-stabilised, cerium-doped

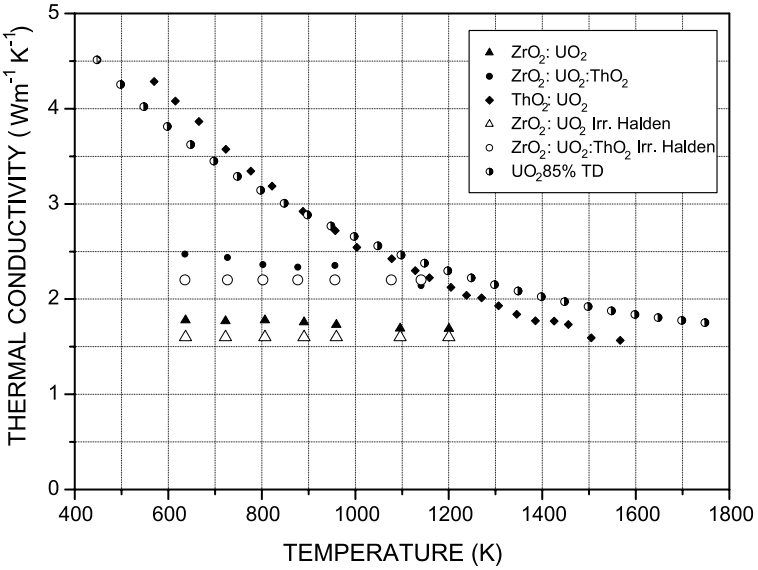

Fig. 10. Thermal conductivity of $(U,Th)O_2$, ZrO_2–UO_2–ThO_2, and ZrO_2–UO_2 versus temperature. For the first two materials the values of λ evaluated after one-month irradiation in the Halden reactor are plotted.

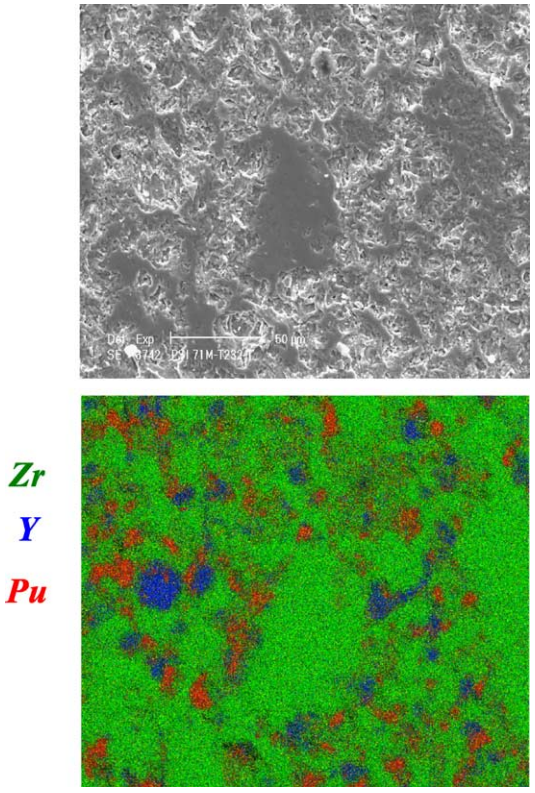

Fig. 11. Structural partition of the components in the Y-st. ZrO_2–PuO_2 composite.

zirconia, fabricated by plasma spraying with the intent of obtaining particularly good refractory and thermal resistance properties. The $\lambda(T)$ curve of this latter, whitish oxide has a positive slope, as in the case of other semitransparent materials, where photon transmission plays an effective role in heat propagation. The same behaviour is observed in both Y- and Ca-stabilised zirconia, whilst the contribution of photon conduction is evidently too small to affect the measured value of λ in the relatively highly conducting monoclinic zirconia.

All mixed or composite oxides are sufficiently optically absorbing to display a negative slope of λ versus T. Yet, this slope is comparatively small, so that at temperatures above approximately 1500 K the conductivity values of all the zirconia-based matrices are not much lower than, for instance, those of UO_2.

A comparative analysis of the physical mechanisms governing heat conduction in the investigated semitransparent materials is not straightforward as it involves complex models and thermo-optical properties which are not sufficiently available. A few general considerations are, however, here in order.

First, the low intrinsic thermal conductivity of cubic zirconia is very likely associated to a large concentration of lattice defects where phonons are very effectively scattered. This is understandable for doped, stabilised zirconia, but it is apparently also an intrinsic property of the pure crystal. An intuitive grasp of this effect can be had from a simple consideration.

Since the transition between the tetragonal form of ZrO_2, stable at low temperatures, and the cubic form occurs through small atomic re-arrangements, the

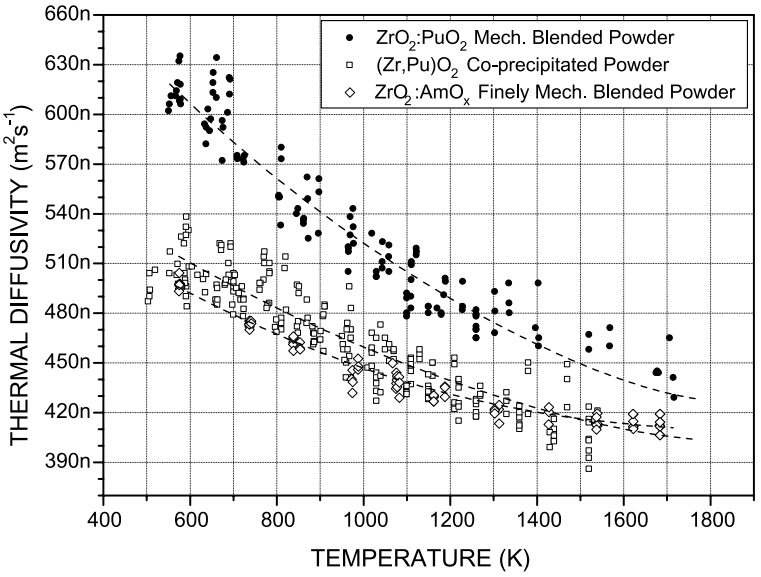

Fig. 12. Thermal diffusivity of Y-st. ZrO_2–PuO_2 composites and Y-st. $(Zr,Pu)O_2$–PuO_2 mixed oxide.

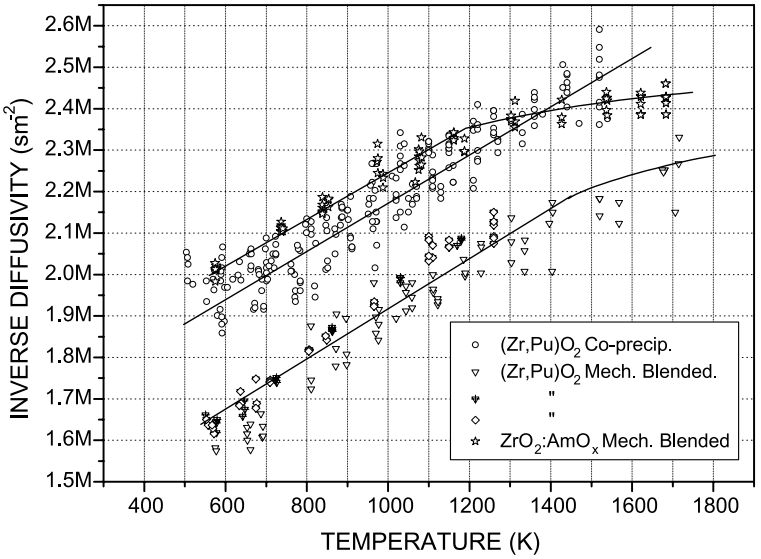

Fig. 13. Inverse diffusivity from the plot of Fig. 11.

existence in the lattice of spatially near, equilibrium configurations [3] can favour local anharmonic effects in lattice vibrations and increase phonon scattering. In the light of this property, an amelioration of the thermal transport of cubic zirconia by improvement of fabrication methods is, therefore, very likely unfeasible.

In our case, the thermal conductivity of zirconia-based matrices becomes worse by adding actinides in solid solution or in finely dispersed, oxide phases. In the latter composites, the experiment has shown that the better conductivity of the globular inclusions does not compensate the negative effect of the poor interface conductance. On the other hand, an improvement in

[3] The energy difference of the two configurations is of the order of 0.13 eV.

thermal conductivity is measured in heterogeneous materials where the actinide phase is present in a sufficiently large volume proportion in the form of a reticulated structure surrounding ZrO_2 clusters. Actually, the positive differential thermal expansion between zirconia and actinide oxides [21] seems to improve the interface conductance at temperatures above 1400 K, where the effective conductivity is approximately 10–20% above the extrapolated value.

We turn finally to the question as to how we can devise an optimisation of IMFs. In heterogeneous composites, there is an obvious plurality of accessible structural patterns with different thermal transport properties where the most advantageous ones for thermal transport under irradiation conditions can be recognised and, possibly, fabricated, as, e.g., the network structures examined above. Yet, there may be fundamental limitations connected with changes brought about by burn-up and long time irradiation, the true extent of which will only become known at the end of the planned irradiation campaign. The results of such analysis would have to mesh with theory and post-irradiation examinations. Whether at root refinement of fabrication methods may significantly improve the in-pile performance of zirconia-based IMFs, we still know not.

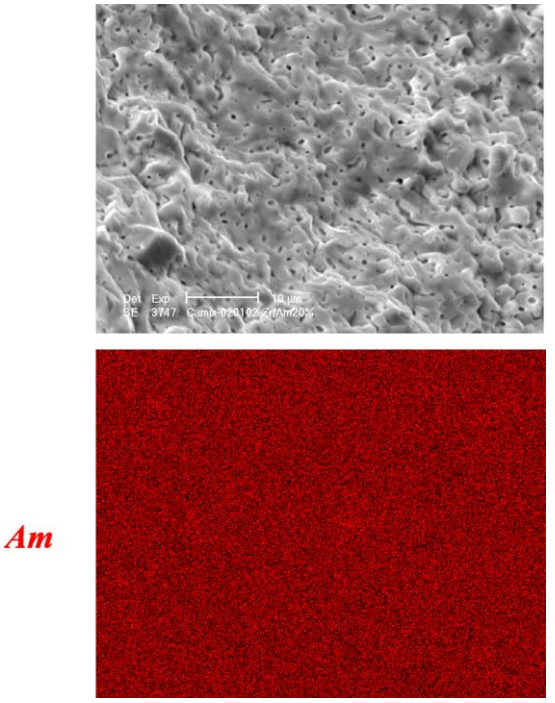

Fig. 14. Structural partition of the components in the Y-st. ZrO_2–AmO_x composite.

Acknowledgements

We are very grateful to the thermophysics staff of ITU, M. Sheindlin, M. Joergensen and G. Pagliosa for the invaluable experimental work performed.

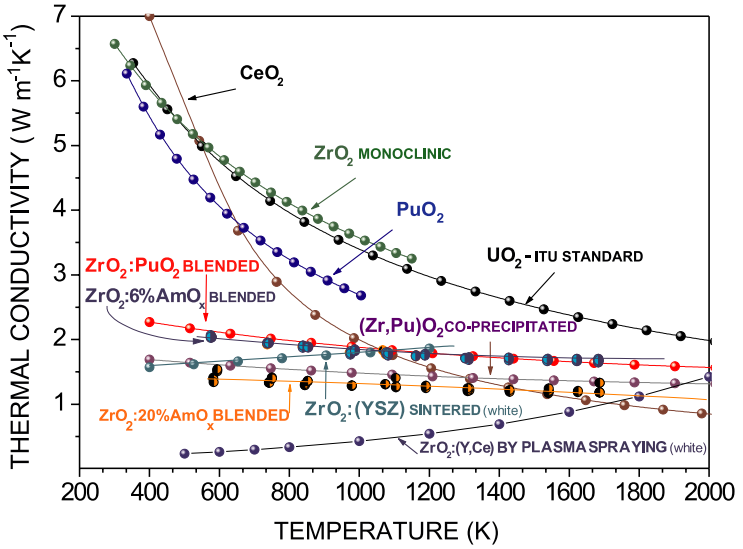

Fig. 15. Synoptic plot of the thermal conductivity of the measured ZrO_2-based IMFs compared to the thermal conductivity of some of the components. Ceria is also included as it is often used as a substitute for plutonia.

References

[1] M. Sheindlin, D. Halton, M. Musella, C. Ronchi, Rev. Sci. Instrum. 69 (3) (1998) 1426.
[2] C.D. Pears, D. Osment, Report ASD-TDR 62-765, (AD 298 061), USA, 1963.
[3] I.B. Fieldhouse, J.I. Lang, Report WADD TR 60-904, USA, 1961.
[4] W.S. Ljaschenko, Metallurgia 10 (11) (1935) 92.
[5] W. Ljaschenko, Metallurgia 11 (1) (1936) 107.
[6] L.B. Pankratz, K.K. Kelley, US Bur. Mines Rep. Invest. 6295 (1963) 1.
[7] A.C. Victor, T.B. Douglas, J. Res. Natl. Bur. Stand. 67A (4) (1963) 325.
[8] Janaf, Supplements, in: D.R. Stull, H. Prophet, (Eds.), Thermophysical Tables, vol. 37, NSRDS-NBS, Washington, p. 1971.
[9] C. Ronchi, M. Sheindlin, J. Appl. Phys. 90 (7) (2001) 3325.
[10] W.A. Lambertson, M.H. Mueller, J. Am. Ceram. Soc. 36 (1953) 365.
[11] G.M. Wolten, J. Am. Ceram. Soc. 80 (1958) 4772.
[12] I. Cohen, B.E. Shaner, J. Nucl. Mater. 9 (1963) 18.
[13] K.A. Romberger, J. Baes, H.H. Stone, J. Inorg. Nucl. Chem. 29 (1967) 1619.
[14] V.Y. Chekhovskoy, A.M. Banaev, in: A.V. Likov (Ed.), Nauka I Tekhnika, vol. VII, Ed. Acad, Minsk, 1968.
[15] P.B. Kantor, Y.N. Fomichov, Tieplovys. Svoist. Tviord Tiel., Soviet Bureau of Standard, Moscow, 1969, p. 406.
[16] J.P. Coughlin, E.G. King, J. Am. Chem. Soc. 72 (1950) 2262.
[17] V.Y. Chekhovskoy, V.Y. Zukhov, V.D. Tarasov, Tepl. Vys. Temp. 17 (4) (1979) 754.
[18] V.A. Kirillin, A.E. Sheindlin, V.Y. Chekhovskoy, I.A. Zhukhova, V.D. Tarasov, Tepl. Vys. Temp. 4 (1966) 878.
[19] R.J. Ackermann, E.G. Rauh, C.A. Alexander, High Temp. Sci. 7 (1975) 304.
[20] T. Tverberg, Report HRP ID: F-NOTE 1746, Halden, 2000.
[21] R. Calabrese, Report JRC-ITU-TPW, 2002-7, European Commission, Karlsruhe, 2002.